Inorganic Chemistry

Article

pubs.acs.org/IC

Diverse Closed Cavities in Condensed Rare Earth Metal–Chalcogenide Matrixes: $Cs[Lu_7Q_{11}]$ and $(ClCs_6)[RE_{21}Q_{34}]$ (RE = Dy, Ho; Q = S, Se, Te)

Hua Lin,[†,‡] Long-Hua Li,[†] and Ling Chen*[,†]

[†]Key Laboratory of Optoelectronic Materials Chemistry and Physics, Fujian Institute of Research on the Structure of Matter, Chinese Academy of Sciences, Fuzhou, Fujian 350002, People's Republic of China

[‡]Graduate University of Chinese Academy of Sciences, Beijing 100039, People's Republic of China

Supporting Information

ABSTRACT: Two types of novel ordered chalcogenids $Cs[Lu_7Q_{11}]$ (Q = S, Se) and $(ClCs_6)[RE_{21}Q_{34}]$ (RE = Dy, Ho; Q = S, Se, Te) were discovered by high-temperature solid state reactions. The structures were characterized by single-crystal X-ray diffraction data. $Cs[Lu_7Q_{11}]$ crystallize in the orthorhombic *Cmca* (no. 64) with a = 15.228(4)−15.849(7) Å, b = 13.357(3)−13.858(6) Å, c = 18.777(5)−19.509(8) Å, and Z = 8. $(ClCs_6)[RE_{21}Q_{34}]$ crystallize in the monoclinic *C*2/*m* (no. 12) with a = 17.127(2)−18.868(2) Å, b = 19.489(2)−21.578(9) Å, c = 12.988(9)−14.356(2) Å, β = 128.604(2)−128.738(4)°, and Z = 2. Both types of compounds feature 3D RE−Q network structures that embed with dual tricapped cubes $Cs_2@Se_{18}$ in the former or unprecedented matryoshka nesting doll structure cavities of $(ClCs_6)@Se_{32}$ in the latter. The band gap, band structure, as well as a structure change trend of the majority of A/RE/Q compounds are presented.

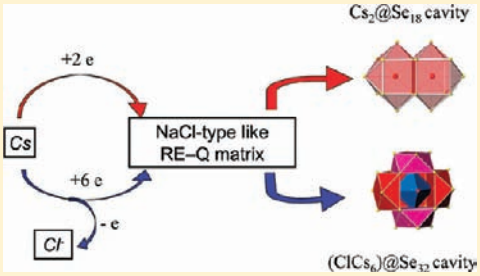

INTRODUCTION

Ternary alkali metal/rare earth metal/chalcogenide compounds (A/RE/Q, Q = S, Se, Te) are fascinating for their complexity and beauty. Up until now, eight types of structures are known and are listed according to their A/RE/Q stoichiometries as following, 1:1:2 (including about 40 compounds, e.g., $RbLaSe_2$),[1−9] 3:7:12 (adopted by roughly 10 compounds, e.g., $Rb_3Yb_7Se_{12}$),[10−15] 1:3:5 (only 2 examples of $CsEr_3Se_5$ and $CsHo_3Te_5$),[16] 3:11:18 (only found in $Cs_3Tm_{11}Te_{18}$),[16] 1:5:8 ($RbSc_5Te_8$),[17] 2:24:36 (as found in a Tm fractional occupied example, $K_2Tm_{23.33}S_{36}$),[18] 1:1:4 (including 12 compounds, e.g., $KCeSe_4$),[19−23] and 1:3:8 (including 4 compounds, e.g., KPr_3Te_8).[22,24,25] Note that 1:1:4 and 1:3:8 types of compounds possess Q−Q bonding interactions and are thus excluded from the structure discussion below. Another exception is $K_2Tm_{23.33}S_{33}$[18] in which two types of building units are found as TmS_6 and TmS_7. All of the remaining A/RE/Q compounds have two structural moieties generally, i.e., the positive moiety, discrete interstitial A cation, and the negative moiety, anionic RE/Q substructure constructed by the REQ_6 octahedron building unit. The structural diversity comes from the rich ways that the building unit REQ_6 can be linked by, such as edge-sharing in layered $RbLuSe_2$,[1] and edge- and face-sharing in 3D channel $Cs_3Tm_{11}Te_{18}$.[16]

The majority of A/RE/Q compounds are channel structure (shown below). Interestingly, the size of the channel increases as the increasing of the A/RE ratio. For example, as the A/RE ratio increases from 0.2 (for $RbSc_5Te_8$ type[17]) to 0.43 (for $A_3RE_7Q_{12}$ type[10−15]), the size of the channel increases which is indicated by the increasing number of A atoms accommodated per channel (e.g., the count of the individual projections of A per channel increase from 1 to 4). Such a trend also fits the layered $AREQ_2$ type structure, if it can be regarded as layers separated by channels with infinite radius. Also the A/RE ratio of the layered structure $AREQ_2$ represents the known upper limit in the A/RE/Q system. To break such an upper limit, i.e., A/RE > 1, requires that each REQ_6 building unit is isolated and surrounded by more than 3 A cations. Such an arrangement will be at least structurally very unstable, and no example has been known yet. However, several oxides are found, for instance, A_2REO_3 features 1D-chains of edge-shared REO_5 square pyramids that are surrounded by A^+ cations,[26] and suboxometallate A_9MO_4, which belongs to a different category.[27] On the other hand, the known A/RE/Q compounds suggest a lower A/RE ratio limit of 0.2, and it will be very interesting to see if the A/RE ratio can be less than 0.2 and under such conditions how the negative REQ_m^{n-} moiety will be organized.

In this paper, two unprecedented types of structures, $Cs[Lu_7Q_{11}]$ (Q = S, Se) and $(ClCs_6)$ $[RE_{21}Q_{34}]$ (RE = Dy, Ho; Q = S, Se, Te), are discovered via high temperature solid state reactions. The A/RE ratio 0.14 for the former breaks the known lower limit, and the negative $[Lu_7Q_{11}]^-$ is no longer an open channel structure, instead, it is a close cavity of dual Cs-centered tricapped cube of $Cs_2@Se_{18}$ periodically embedded

Received: November 20, 2011
Published: March 26, 2012

   dx.doi.org/10.1021/ic202494w | *Inorg. Chem.* 2012, 51, 4588−4596

within the Lu_7Q_{11} covalent bond matrix. Also for the latter, the A/RE ratio 0.29 lies between the known 0.27 ($A_3RE_{11}Q_{18}$ type) and 0.33 (ARE_3Q_5 type), and the negative moiety is not an open channel structure but a matryoshka nesting doll structure cavity of $(ClCs_6)@Se_{32}$ embedded within the $RE_{21}Q_{34}$ matrix. The syntheses, single crystal analyses, optical band gap, as well as electronic structures based on VASP calculations are reported.

EXPERIMENTAL SECTION

Syntheses. Reactants were stored in an Ar-filled glovebox with controlled oxygen and moisture levels below 0.1 ppm. Chunks of Dy, Ho, and Lu, (99.95%) were purchased from Huhhot Jinrui Rare Earth Co., Ltd. Powdery or lumpy S, Se, and Te (99.999%) were purchased from Alfa Aesar, and powdery CsCl (99.99%) was purchased from Sinopharm Chemical Reagent Co., Ltd. Reactants were put in evacuated fused-silica tubes and annealed in tube furnaces with controlled temperature.

$Cs[Lu_7Se_{11}]$. After numerous explorations on the experimental conditions including starting reactant, loading ratio, annealing temperature, the optimal synthesis condition was established as loading a stoichiometry mixture (about 300 mg in total) of CsCl, Lu, and Se in a molar ratio of 1:7:11 in a fused-silica tube under vacuum, annealing at 723 K for 1 day and then 1223 K for 4 days followed by cooling to 473 K at 5 K/h before switching off the furnace. Dark-red irregular plate crystals with good quality were subsequently selected for single crystal X-ray diffraction studies. The EDX results confirmed the presence of Cs, Lu, and Se in an approximate molar ratio of $Cs_{1.0}Lu_{7.0(4)}Se_{11.0(3)}$ (Supporting Information, Figure S1). The products with a yield of about 95% were washed with ethanol to remove the soluble byproduct, dried in air, and after this treatment, pure phased, dark-red crystals of $Cs[Lu_7Se_{11}]$ were obtained according to the XRD pattern shown in Figure 1a.

$Cs[Lu_7S_{11}]$. Accordingly, the optimal synthesis condition of the sulfur analogue was established. The only difference is the loading ratio was CsCl/Lu/S = 2:7:11 (with a slight excess of CsCl) and the reaction yield was about 85%. After washing with EtOH and sieving, pure phased, red crystals of $Cs[Lu_7S_{11}]$ were obtained (Figure 1b).

These compounds were stable in air for several months. $Cs[Lu_7S_{11}]$ was insoluble in water, but $Cs[Lu_7Se_{11}]$ decomposed in water.

Series reactions had been loaded to probe the role of CsCl. Also we found the amount of CsCl was crucial. For sulfide, the loading ratios of CsCl/Lu/S = 1:7:11 and 2:7:11 can generate the target compound at yields of 25 and 85%, respectively. Other loading ratios, such as 4:7:11, 6:7:11, and 8:7:11, mostly produced CsCl and Lu_2S_3, and no target ternary compound was observed. For the selenide analogue, except for the stoichiometric reaction, other loading ratios mostly produce CsCl and binary Lu_2Se_3 under the experimental conditions.

$(ClCs_6)[RE_{21}Q_{34}]$ (RE = Dy, Ho; Q = S, Se, Te). These compounds were obtained from mixtures of stoichiometric CsCl/RE/Q = 6:21:34 in evacuated silica tubes by heating to 1223 K over 100 h, maintaining there for 120 h and cooling to 473 K at 4 K/h before switching off the furnace. Block crystals with good quality were obtained, and the single crystal X-ray diffraction data $(ClCs_6)[RE_{21}Q_{34}]$ agreed well with the EDX analysis results, e.g., $Cs_6Ho_{21.3(2)}Se_{34.0(3)}Cl_{1.0(2)}$ (Supporting Information, Figure S2). In general, $(ClCs_6)[RE_{21}Q_{34}]$ was extremely more difficult to synthesize than $Cs[Lu_7Q_{11}]$. As shown in Figure 1c, nearly pure phased $(ClCs_6)[Ho_{21}Se_{34}]$ crystals were obtained after washing with absolute ethanol. $(ClCs_6)[RE_{21}Q_{34}]$ is very sensitive to air, and quick decomposition was observed shortly after its exposure (Figures S3 and S4 in the Supporting Information).

Crystal Structure Determinations. Diffraction data were collected on a Rigaku Mercury CCD diffractometer or a Rigaku Saturn724 CCD diffractometer equipped with graphite-monochromated Mo Kα radiation (λ = 0.710 73 Å) at 293 K. The $Cs[Lu_7Q_{11}]$ crystals are mounted on glass fibers with glue for structure determination, whereas $(ClCs_6)[RE_{21}Se_{34}]$ crystals are sealed inside a glass capillary (i.d. 0.3 mm). The data were corrected for the Lorentz and polarization factors. The absorption corrections were based on the multiscan method.[28] All structures were solved by the direct methods and refined by the full-matrix least-squares fitting on F^2 by SHELX-97.[29] All atoms were refined with anisotropic thermal parameters. The coordinates were standardized using STRUCTURE TIDY.[30]

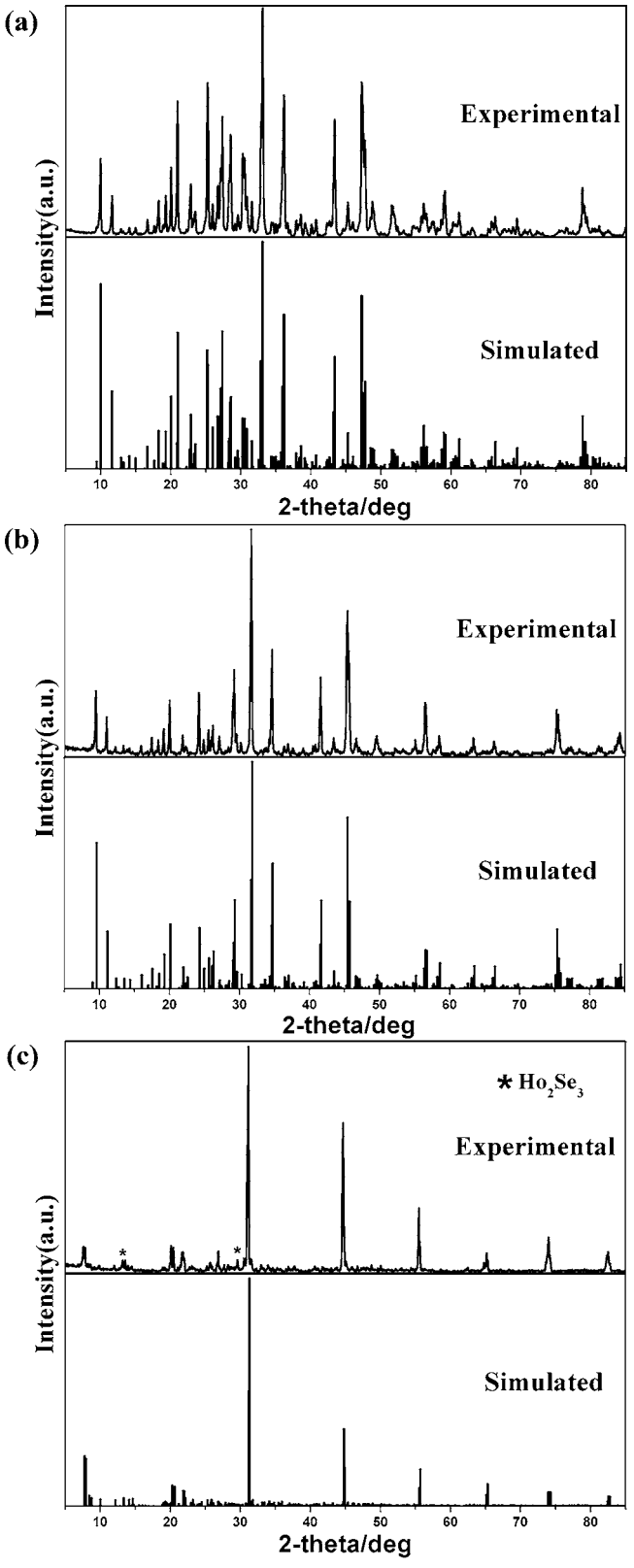

Figure 1. The experimental and simulated X-ray powder diffraction patterns of (a) $Cs[Lu_7S_{11}]$, (b) $Cs[Lu_7Se_{11}]$, and (c) $(ClCs_6)[Ho_{21}Se_{34}]$.

dx.doi.org/10.1021/ic202494w | Inorg. Chem. 2012, 51, 4588–4596

As listed in Tables 2–4, Cs sites in both types of compounds invariably exhibit large displacement parameters (3–5 times larger than those of RE and Q atoms). With $CsLu_7Se_{11}$ as an example, free occupancy refinement on the Cs sites converged to nearly 100% with similar U(eq) = 0.0358(4), $R1$ (0.0424), and wR2 (0.0876). As discussed below, the Cs cations are centered on a dual tricapped cube of Se_{18} with a volume of 5.7 × 8.0 × 11.6 Å^3; thus, it might behave as a rattling atom so as to exhibit large thermal parameters. The single crystal stoichiometry was confirmed by the EDX results $Cs_{1.0}Lu_{7.0(4)}Se_{11.0(3)}$. The structures were solved without events. The refined stoichiometry was in good agreement with the EDX results $Cs_{6.0}Ho_{21.3(2)}Se_{34.0(3)}Cl_{1.0(2)}$. Crystallographic data and structural refinement details are summarized in Table 1, the positional coordinates and isotropic equivalent thermal parameters are given in Tables 2–4, and important bond distances are listed in Table 5. More details of the crystallographic studies are given as Supporting Information.

Table 1. Crystallographic Data and Refinement Details for $Cs[Lu_7Q_{11}]$ and $(ClCs_6)$ $[Dy_{21}Se_{34}]$

formula	$Cs[Lu_7S_{11}]$	$Cs[Lu_7Se_{11}]$	$(ClCs_6)$ $[Dy_{21}Se_{34}]$
Fw	1710.36	2226.26	6930.05
temperature (K)	293(2)	293(2)	293(2)
crystal system	orthorhombic		monoclinic
space group	*Cmca* (no. 64)		*C*2/*m* (no. 12)
Pearson symbol	*oC152*		*mC124*
a (Å)	15.228(4)	15.849(7)	17.787(7)
b (Å)	13.357(3)	13.858(6)	20.290(7)
c (Å)	18.777(5)	19.509(8)	13.484(6)
α (deg)	90	90	90
β (deg)	90	90	128.686(5)
γ (deg)	90	90	90
V (Å^3)	3820(2)	4285(3)	3799(3)
Z	8	8	2
D_c (g cm^{-3})	5.949	6.902	6.059
μ (mm^{-1})	38.883	52.277	39.525
independent reflns	2271 (R_{int} = 0.0806)	2557 (R_{int} = 0.0703)	3432 (R_{int} = 0.0538)
GOF on F^2	1.157	1.058	1.163
R_1, wR_2 ($I > 2\sigma(I)$)[a]	0.0381, 0.0982	0.0424, 0.0876	0.0409, 0.1024
R_1, wR_2 (all data)	0.0456, 0.1174	0.0557, 0.0972	0.0439, 0.1045
diff peak, hole (e, Å^{-3})	3.691, −3.257	2.487, −2.615	2.095, −3.046

[a] $R_1 = \Sigma||F_o| - |F_c||/\Sigma|F_o|$, $wR_2 = [\Sigma w(F_o^2 - F_c^2)^2/\Sigma w(F_o^2)^2]^{1/2}$.

X-ray Powder Diffraction. The XRD patterns were taken at room temperature on a Rigaku DMAX 2500 powder X-ray diffractometer by using Cu Kα radiation (λ = 1.5406 Å) at room temperature in the range of 2θ = 5–85° with a scan step width of 0.05°. As shown in Figure 1, $Cs[Lu_7Q_{11}]$ were produced with high yields (85% or higher), but the yields of $(ClCs_6)[RE_{21}Q_{34}]$ were low (less than 20%), although washing with ethanol could wash off most of the byproducts so as to give a nearly pure phased $(ClCs_6)[Ho_{21}Se_{34}]$ (Figure 1c).

Elemental Analysis. Spectra were collected on a field emission scanning electron microscope (FESEM, JSM6700F) equipped with an energy dispersive X-ray spectroscope (EDX, Oxford INCA) on clean single crystal surfaces. The results were $Cs_{1.0}Lu_{7.0(4)}Se_{11.0(3)}$ and $Cs_{6.0}Ho_{21.3(2)}Se_{34.0(3)}Cl_{1.0(2)}$ (Figures S1 and S2 in the Supporting Information).

UV–Visible–Near IR Spectroscopies. Since $(ClCs_6)[RE_{21}Q_{34}]$ were very sensitive to air, only optical diffuse reflectance spectra of $Cs[Lu_7Q_{11}]$ powder samples were measured at room temperature using a Perkin-Elmer Lambda 900 UV–vis spectrophotometer equipped with an integrating sphere attachment and $BaSO_4$ as a reference in the range of 0.19–2.5 μm (Figure S5 in the Supporting Information). The absorption spectrum was calculated from the reflection spectrum via the Kubelka–Munk function: $\alpha/S = (1 - R)^2/2R$, in which α was the absorption coefficient, S was the scattering coefficient, and R was the reflectance.[31]

Electronic Structure Calculations. The electronic band structures were calculated by the Vienna ab initio simulation package (VASP).[32,33] The generalized gradient approximation (GGA)[34] was chosen as the exchange-correlation functional, and a plane wave basis with the projector augmented wave (PAW) potentials was used.[35,36] The plane-wave cutoff energy of 230 eV and the threshold of 10^{-5} eV were set for the self-consistent-field convergence of the total electronic energy. The 4*f* electrons of the RE element were treated as core electrons, and the valence electrons were Cs, $6s^1$; Se, $4s^24p^4$; S, $3s^23p^4$; and Cl, $3s^23p^5$. The *k* integration over the Brillouin zone was performed by the tetrahedron method[37] using a 3 × 3 × 1 Monkhorst-Pack mesh, and the Fermi level (E_F = 0 eV) was selected as the reference of the energy.

RESULTS AND DISCUSSION

Crystal Structure. *$Cs[Lu_7Q_{11}]$ (Q = S, Se).* $Cs[Lu_7Q_{11}]$ represents a novel structure type crystallizing in *Cmca* with novel closed dual tricapped $Cs_2@Se_{18}$ cube cavities far apart within the $[Lu_7Q_{11}]^-$ covalent bonding matrix. Each Lu atom is 6-fold coordinated in a distorted $LuSe_6$ octahedron that is packed in a quasi-NaCl type manner along the *c* axis as shown in Figure 2. The symmetry breaking is caused by the distortion

Table 2. Atomic Coordinates and Equivalent Isotropic Displacement Parameters of $Cs[Lu_7S_{11}]$

atom	Wyckoff site	*x*	*y*	*z*	U(eq)[a]
Cs1	8*f*	0	0.4104(2)	0.09110(9)	0.0348(4)
Lu1	8*f*	0	0.09691(5)	0.17585(4)	0.0084(2)
Lu2	16*g*	0.12706(4)	0.32572(4)	0.32647(3)	0.0094(2)
Lu3	8*d*	0.12324(5)	0	0	0.0092(2)
Lu4	16*g*	0.25685(4)	0.07947(4)	0.15893(3)	0.0091(2)
Lu5	8*c*	0.25	0.25	0	0.0087(2)
S1	16*g*	0.1264(2)	0.1603(2)	0.0822(2)	0.0090(7)
S2	16*g*	0.1295(2)	0.0023(2)	0.2450(2)	0.0095(7)
S3	16*g*	0.2562(2)	0.4138(2)	0.0823(2)	0.0112(7)
S4	16*g*	0.3723(2)	0.1727(2)	0.0835(2)	0.0104(7)
S5	8*f*	0	0.2637(4)	0.2460(2)	0.012(2)
S6	8*f*	0	0.4258(3)	0.4089(2)	0.0075(9)
S7	8*e*	0.25	0.2362(3)	0.25	0.013(2)

[a] U_{eq} is defined as one third of the trace of the orthogonalized U_{ij} tensor.

dx.doi.org/10.1021/ic202494w | Inorg. Chem. 2012, 51, 4588–4596

Table 3. Atomic Coordinates and Equivalent Isotropic Displacement Parameters of $Cs[Lu_7Se_{11}]$

atom	Wyckoff site	x	y	z	$U(eq)^a$
Cs1	8*f*	0	0.4131(2)	0.09313(8)	0.0358(4)
Lu1	8*f*	0	0.09527(5)	0.17535(4)	0.0058(2)
Lu2	16*g*	0.12658(3)	0.32584(3)	0.32806(3)	0.0066(2)
Lu3	8*d*	0.12475(5)	0	0	0.0065(2)
Lu4	16*g*	0.25437(3)	0.08156(3)	0.15947(3)	0.0063(2)
Lu5	8*c*	0.25	0.25	0	0.0056(2)
Se1	16*g*	0.12438(7)	0.16341(8)	0.08183(6)	0.0062(3)
Se2	16*g*	0.12883(7)	0.00151(9)	0.24677(6)	0.0059(3)
Se3	16*g*	0.25324(7)	0.41394(8)	0.08299(6)	0.0061(2)
Se4	16*g*	0.37363(7)	0.17031(8)	0.08249(6)	0.0074(3)
Se5	8*f*	0	0.2630(2)	0.24587(9)	0.0101(4)
Se6	8*f*	0	0.4244(2)	0.41044(8)	0.0052(3)
Se7	8*e*	0.25	0.2395(2)	0.25	0.0070(4)

$^a U_{eq}$ is defined as one third of the trace of the orthogonalized U_{ij} tensor.

Table 4. Atomic Coordinates and Equivalent Isotropic Displacement Parameters of "$(ClCs_6)[Dy_{21}Se_{34}]$

atom	Wyckoff site	x	y	z	$U(eq)^a$
Cs1	8*j*	0.42689(6)	0.37930(5)	0.27375(8)	0.0334(2)
Cs2	4*i*	0.27350(8)	0.5	0.4195(2)	0.0341(3)
Dy1	4*g*	0	0.30105(4)	0	0.0176(2)
Dy2	8*j*	0.25321(4)	0.20752(3)	0.24935(5)	0.0120(2)
Dy3	8*j*	0.12817(3)	0.29890(3)	0.37654(5)	0.0119(2)
Dy4	4*g*	0	0.09907(4)	0	0.0117(2)
Dy5	8*j*	0.36556(4)	0.10180(3)	0.10864(5)	0.0122(2)
Dy6	4*h*	0.5	0.10099(4)	0.5	0.0130(2)
Dy7	2*b*	0	0.5	0	0.0122(2)
Dy8	4*i*	0.24341(5)	0	0.25425(7)	0.0117(2)
Se1	4*i*	0.1868(2)	0.5	0.0646(2)	0.0137(4)
Se2	4*i*	0.0588(2)	0	0.1843(2)	0.0127(4)
Se3	8*j*	0.18852(8)	0.10042(6)	0.0716(2)	0.0123(3)
Se4	8*j*	0.18397(8)	0.30083(6)	0.0629(2)	0.0213(3)
Se5	8*j*	0.06719(8)	0.20167(6)	0.1861(2)	0.0124(3)
Se6	8*j*	0.43886(7)	0.19610(6)	0.3106(2)	0.0117(3)
Se7	8*j*	0.31321(8)	0.30047(6)	0.4422(2)	0.0134(3)
Se8	8*j*	0.31585(8)	0.10299(5)	0.4373(2)	0.0119(3)
Se9	8*j*	0.05488(8)	0.39981(6)	0.1841(2)	0.0124(3)
Se10	4*i*	0.4293(2)	0	0.3078(2)	0.0107(3)
Cl1	2*c*	0.5	0.5	0.5	0.034(2)

$^a U_{eq}$ is defined as one third of the trace of the orthogonalized U_{ij} tensor.

of $LuSe_6$ octahedron and the involvement of Cs atoms (red atoms in Figure 2). The Lu−Se bond ranging from 2.701(2) to 2.911(1) Å is comparable to that in $RbLuSe_2$ (2.8371(7) Å)[1] and indicates a strong covalent bonding interaction, and the Se−Lu−Se angle deviates from 90 and 180° considerably (83.7−98.4° and 168−180°) (Table 5). The five crystallographically independent Lu atoms are arranged in two basic layers denoted as layer A (by Lu3 and Lu5) and layer B (Lu1, Lu2, Lu4). As indicated in Figure 2, the 2-fold screw axis operates layer A into layer A^{2_1} and layer B into B^{2_1}. Layer $B^{2_1, i}$ has been generated from Layer B by the 2-fold screw axis and the center of symmetry operations, and so on and so forth. Eventually, Lu atoms are stacking along the *c* direction in a sequence of (...A, B, B^{2_1}, A^{2_1}, $B^{2_1, i}$, B^i, A...).

Unprecedently, the $[Lu_7Se_{11}]^-$ covalent bond matrix accommodates large Cs-centered cavities as indicated in Figure 3, and green lines in Figure 2 indicate the orientations of such cavities. Because of the involvement of Cs cations, the packing density of $Cs[Lu_7Se_{11}]$ is lower than the NaCl type LuSe,[38] which is reflected by the lower coordination numbers (CN). In $Cs[Lu_7Se_{11}]$, the CN of Se atoms (3, 4, or 5) are lower than 6 in the NaCl type but higher than 3 in Al_2O_3-type Lu_2Se_3.[39] In more detail, as the black ball in Figure 3 indicated, Se6 and Se7 are not involved to construct the $Cs_2@Se_{18}$ cavity, Se6 is 5-fold coordinated in a distorted $SeLu_5$ square pyramid with the Lu−Se bond varying from 2.84 to 2.91 Å, while Se7 is 4-fold coordinated in a distorted tetrahedron (Figure S6 in the Supporting Information). Directed by the electrostatic interaction between Cs^+ cations and Se^{2-} anions, the Se1-, Se2-, Se3-cis-divacant octahedra together with Se4-triangular pyramid and Se5-nearly coplanar triangle envelope two isolated Cs^+ cations to form a closed cavity of a dual tricapped cube, $Cs_2@Se_{18}$, which is at least 10.5 Å apart within the matrix of the $[Lu_7Se_{11}]^{2-}$ moiety (Figures 3 and 4). Such a discrete Se_{18} dual tricapped cube is observed for the first time. Note that the formal description of the cavity polyhedron does not imply anything about bonding. A related omnicapped cube of the Ge_{14}^{2-} cluster[40] has been observed, of which the dimerization

dx.doi.org/10.1021/ic202494w | Inorg. Chem. 2012, 51, 4588−4596

Table 5. Selected Bond Lengths (Å) of $Cs[Lu_7Q_{11}]$

	$Cs[Lu_7S_{11}]$	$Cs[Lu_7Se_{11}]$		$Cs[Lu_7S_{11}]$	$Cs[Lu_7Se_{11}]$
Cs1–Q1 × 2	3.858(3)	3.988(2)	Q1–Lu1	2.742(3)	2.848(2)
Cs1–Q2 × 2	3.857(4)	3.928(2)	Q1–Lu4	2.682(3)	2.798(2)
Cs1–Q3 × 2	3.905(4)	4.018(2)	Q1–Lu3	2.640(3)	2.771(2)
Cs1–Q4 × 2	3.969(4)	4.094(2)	Q1–Lu5	2.713(3)	2.821(2)
Cs1–Q4 × 2	4.010(3)	4.133(2)	Q2–Lu1	2.677(3)	2.793(2)
Cs1–Q5	3.507(5)	3.634(3)	Q2–Lu2	2.713(3)	2.839(2)
Lu1–Q1 × 2	2.742(3)	2.848(2)	Q2–Lu4	2.706(3)	2.830(2)
Lu1–Q2 × 2	2.677(3)	2.793(2)	Q2–Lu4	2.726(3)	2.845(2)
Lu1–Q5	2.589(5)	2.701(2)	Q3–Lu2	2.735(4)	2.852(2)
Lu1–Q6	2.785(5)	2.901(2)	Q3–Lu3	2.661(3)	2.790(2)
Lu2–Q2	2.713(3)	2.839(2)	Q3–Lu4	2.647(3)	2.764(2)
Lu2–Q3	2.735(4)	2.852(2)	Q3–Lu5	2.680(3)	2.791(2)
Lu2–Q4	2.653(3)	2.774(2)	Q4–Lu2	2.653(3)	2.774(2)
Lu2–Q5	2.590(3)	2.712(2)	Q4–Lu4	2.579(3)	2.710(2)
Lu2–Q6	2.816(3)	2.911(1)	Q4–Lu5	2.644(3)	2.766(2)
Lu2–Q7	2.645(2)	2.754(2)	Q5–Lu1	2.589(5)	2.701(2)
Lu3–Q1 × 2	2.640(3)	2.771(2)	Q5–Lu2 × 2	2.590(3)	2.712(2)
Lu3–Q3 × 2	2.661(3)	2.790(2)	Q6–Lu1	2.785(5)	2.901(2)
Lu3–Q6 × 2	2.726(3)	2.840(2)	Q6–Lu2 × 2	2.816(3)	2.911(1)
Lu4–Q1	2.682(3)	2.798(2)	Q6–Lu3 × 2	2.726(3)	2.840(2)
Lu4–Q2	2.706(3)	2.830(2)	Q7–Lu2 × 2	2.645(2)	2.754(2)
Lu4–Q2	2.726(3)	2.845(2)	Q7–Lu4 × 2	2.705(3)	2.813(2)
Lu4–Q3	2.647(3)	2.764(2)			
Lu4–Q4	2.579(3)	2.710(2)			
Lu4–Q7	2.705(3)	2.813(2)			
Lu5–Q1 × 2	2.713(3)	2.821(2)			
Lu5–Q3 × 2	2.680(3)	2.791(2)			
Lu5–Q4 × 2	2.644(3)	2.766(2)			

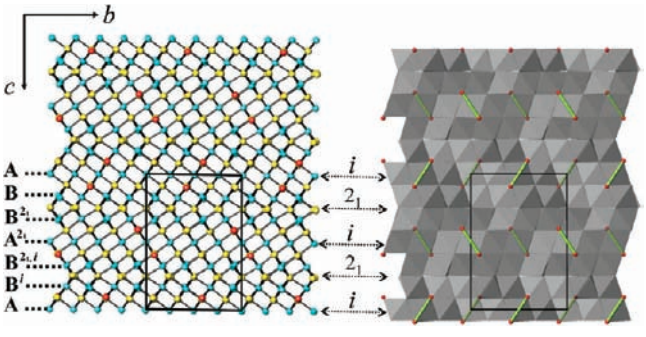

Figure 2. (left) Structure and (right) octahedron packing of $Cs[Lu_7Se_{11}]$ viewed down the *c*-direction with the unit cell marked. Red, Cs; blue, Lu; yellow, Se; gray octahedron, $LuSe_6$; green line, Cs–Cs distance. The (...A, B, B^{2_1}, A^{2_1}, $B^{2_1,i}$, B^{i}, A...) packing sequence of the Lu metals is labelled on the left. The major symmetry element (*i*, center of symmetry; 2_1, 2-fold screw axis at c = 0, 1/4, 1/2, 3/4, respectively) is marked in the middle.

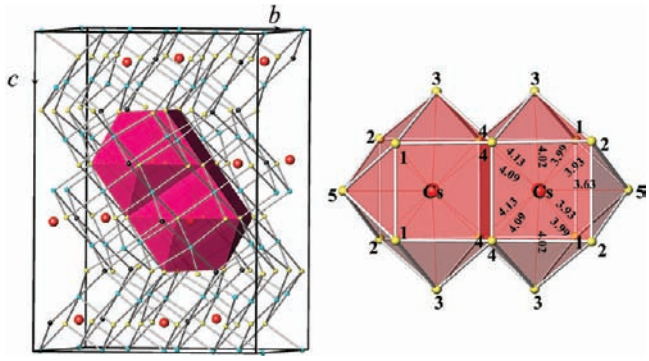

Figure 3. (left) The unit cell of $Cs[Lu_7Se_{11}]$ emphasizing the large closed Cs-centered cavity (purple pholyhedron) embedded in the matrix of Lu–Se bonds (less than 3.0 Å). Red, Cs; blue, Lu; yellow, Se1–5; black, Se6, 7. (right) The view of the $Cs_2@Se_{18}$ dual tricapped cube with the atom number and Cs–Se distance marked.

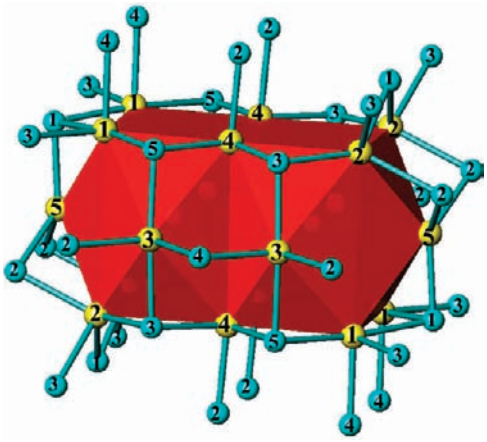

Figure 4. The dual tricapped $Cs_2@Se_{18}$ cube enveloped by Se1–5 anions with each Se-coordination polyhedron outlined. Yellow, Se; blue, Lu. Se1, Se2, Se3 are 4-fold coordinated in cis-divacant octahedra with their vacant sites facing the Cs^+ center. The 3-fold coordinated Se4 and Se5 are in triangular pyramids and a nearly coplanar triangle, respectively.

may give rise to the dual tricapped cube found here. Of course, the differences are obvious, for instance, the Se_{18} polyhedron is centered by two isolated Cs^+ cations but the Ge_{14}^{2-} cube is empty, and the Ge–Ge bonding is strong but no Se–Se interaction is suggested. The Cs–Se distances range from 3.634(3) to 4.133(2) Å with an average of 4.014 Å slightly larger than the sum of the ionic radii (3.86 Å, r_{Cs}^{+} = 1.88 Å for CN = 12 and r_{Se}^{2-} = 1.98 Å for CN = 6),[41] which indicates a large thermal vibration of the Cs atom. As a result, the thermal parameters of Cs are rather large (U(eq) = 0.0358 for Cs1, roughly 5–6 times larger than those of Lu atoms). As the pair of cubes of $Cs_2@Se_{18}$ share common faces, the centering cation–cation repulsion results in the short Cs–Se5 distances (3.634(3) Å), which consist of those in $CsEr_3Se_5$ (3.618(3)–3.819(3) Å).[11]

$(ClCs_6)[RE_{21}Q_{34}]$ (RE = Dy, Ho; Q = S, Se, Te). Different from the discussion above, it is amazing that an octahedron of $ClCs_6$ can also serve as the center species in a closed cavity of $(ClCs_6)@Se_{32}$, which is distributed with a large interval, at least 13.5 Å apart, in the RE–Q matrix in $(ClCs_6)[RE_{21}Q_{34}]$ compounds.

The unit cell of $(ClCs_6)[Dy_{21}Se_{34}]$ is shown in Figure 5. The same as in $Cs[Lu_7Se_{11}]$, all Dy atoms are 6-fold coordinated in

dx.doi.org/10.1021/ic202494w | Inorg. Chem. 2012, 51, 4588–4596

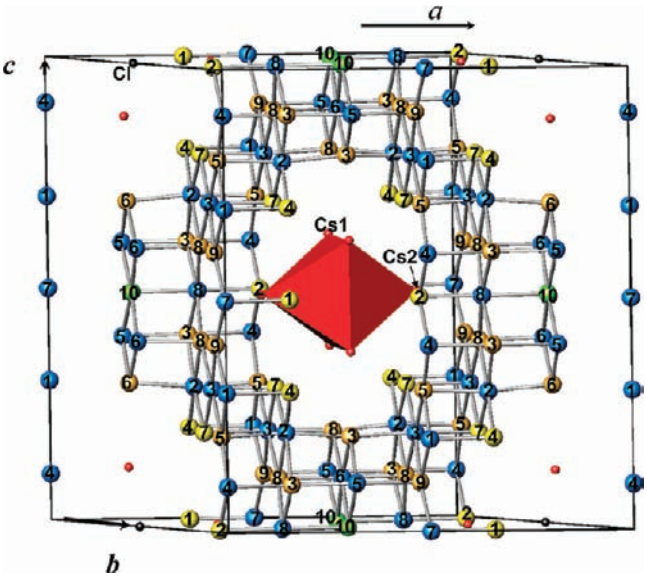

Figure 5. The unit cell of $(ClCs_6)[Dy_{21}Se_{34}]$ with the imbedded $ClCs_6$ octahedron outlined (red). The atom number and unit cell are marked, and Dy−Se bonds are less than 3.0 Å. Red, Cs; blue, Dy; and black, Cl. Yellow, 3-fold coordinated Se1, Se2, Se4, Se7 in triangular pyramids. Orange yellow, 4-fold coordinated Se3, Se5, Se6, Se8, Se9 in cis-divacant octahedra; green, 5-fold coordinated Se10 in a square pyramid.

distorted $DySe_6$ octahedra with Dy−Se bonds ranging from 2.735(2) to 2.994(2) Å, which are also comparable to those in $Cs[Lu_7Se_{11}]$, 2.824−2.981 Å in $Rb_3Dy_7Se_{12}$,[15] and 2.846 Å in $LiDySe_2$,[2] as well as the sum of the ionic radii for Se^{2-} and Dy^{3+} (2.892 Å).[41] The Se−Dy−Se angular deviations are also similar as those in $Cs[Lu_7Se_{11}]$, ranging from 84.7 to 96.9° and 171 to 180°, respectively (Table S8 in the Supporting Information). Besides, CN of Se atoms are 3, 4, and 5 as well, but the arrangement of the Se atoms is totally different (Figure 5). In comparison, the Se_{18} polyhedron in $Cs[Lu_7Se_{11}]$, a pair of Cs atoms centered dual-tricapped cube, defines a closed cavity boundary within the negative Lu_7Se_{11} matrix (Figures 3 and 4). Whereas in $(ClCs_6)[Dy_{21}Se_{34}]$, the negative cavity boundary has been confined by the Se_{32} matryoshka nesting doll structure polyhedron centered by an octahedron $ClCs_6$ (Figure 7). Such cavities are at least 13.5 Å apart and are distributed within the quasi-NaCl type $[Dy_{21}Se_{34}]^{5-}$ matrix (Figure 6). Because the cavity $(ClCs_6)@Se_{32}@[Dy_{21}Se_{34}]$ (about 12 × 12 × 12 Å^3) is larger than $Cs_2@Se_{18}@[Lu_7Se_{11}]_2$ (about 6 × 8 × 12 Å^3), the density of $(ClCs_6)[Dy_{21}Se_{34}]$ is significantly lower than $Cs[Lu_7Se_{11}]$, 6.06 vs 6.90 g cm^{-3} (Table 1). Interestingly, only 3- and 4-fold coordinated Se atoms are involved to confine the cavity in both types of compounds. For instance, the 5-fold coordinated Se10 atoms in $(ClCs_6)[Dy_{21}Se_{34}]$ are excluded to confine the $(ClCs_6)@Se_{32}$ matryoshka nesting doll structure cavities (Figures 5 and 7)

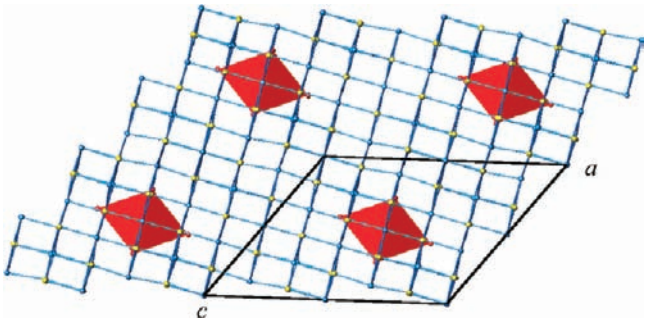

Figure 6. Structure of $(ClCs_6)(Dy_{21}Se_{34})$ viewed down the *b*-direction showing a quasi-NaCl type-DySe matrix formed by 6-folded coordinated Dy metals with Dy−Se bonds less than 3.0 Å. The discrete $ClCs_6$ octahedra (red) are embedded in such a matrix. Blue, Dy; yellow, Se.

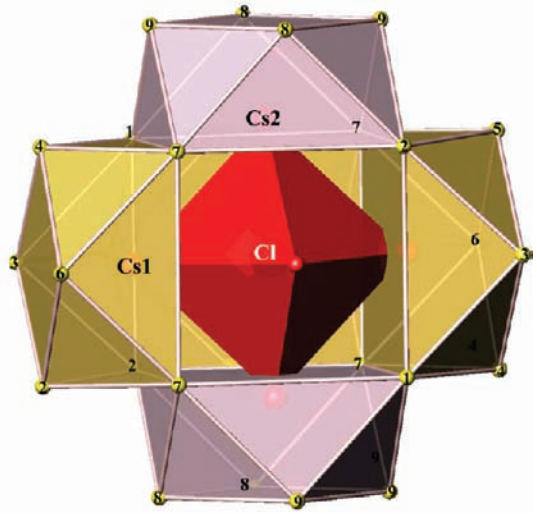

Figure 7. The matryoshka nesting doll structure. The $ClCs_6$ octahedron is surround by four Cs1 centered- and two Cs2 centered-square antiprisms. The front Cs1-antiprism is omitted for a better view. Yellow: Se with atom number marked.

The Cs−Cl bond lengths vary in the range of 3.456(2)−3.470(2) Å, which are consistent with those observed in CsCl (3.461 Å)[42] and Cs_2YbCl_4 (3.441−3.837 Å).[43] The Cs−Se bond lengths fall in the range of 3.729 (2) to 4.189 (2) Å, in good agreement with those in $Cs[Lu_7Se_{11}]$ discussed above.

It is very interesting to compare the two charge-balanced formulas, $(Cs^+)[(Lu^{3+})_7(Se^{2-})_{11}]^-$ vs $(ClCs_6)^{5+}[(Dy^{3+})_{21}(Se^{2-})_{34}]^{5-}$, which suggests that the electron accommodation ability of the quasi-NaCl type RE−Se bonding matrix is quite flexible.

Comparison with Other Ternary A/RE/Q Systems. The major A/RE/Q structure types have been shown in Figure 8, which has nicely displayed a correlation between the structure and the A/RE atomic ratio. As discussed briefly in the Introduction, as the A/RE atomic ratio increases from 0.14 ($Cs[Lu_7Q_{11}]$) to 1 ($AREQ_2$ type[1−9]), the structure varies from a closed cavity structure to an open channel structure and then to a 2D layered structure. Such a trend goes roughly monotonically with the density decrease (identity of atom should be taken into account). For instance, in spite of the closed cavity structural feature of $(ClCs_6)[Dy_{21}Se_{34}]$, the A/RE ratio (3/10.5 = 0.29) and density (6.06 g cm^{-3}) are located between those of $Cs_3Tm_{11}Te_{18}$[16] and $Cs_3Y_7Se_{12}$[12] (6.67 and 4.73 g cm^{-3}), suggesting a quite loose packing because of the large cavity, which agrees well with the structure feature discussed above. Therefore, this compound also fits in such an A/RE ratio-structure change trend. The packing density can be roughly probed by the size of the open channel/cavity in the compound. The larger the channel/cavity is, the less condensed the structure is. The 2D layered structure can be regarded as a

dx.doi.org/10.1021/ic202494w | Inorg. Chem. 2012, 51, 4588−4596

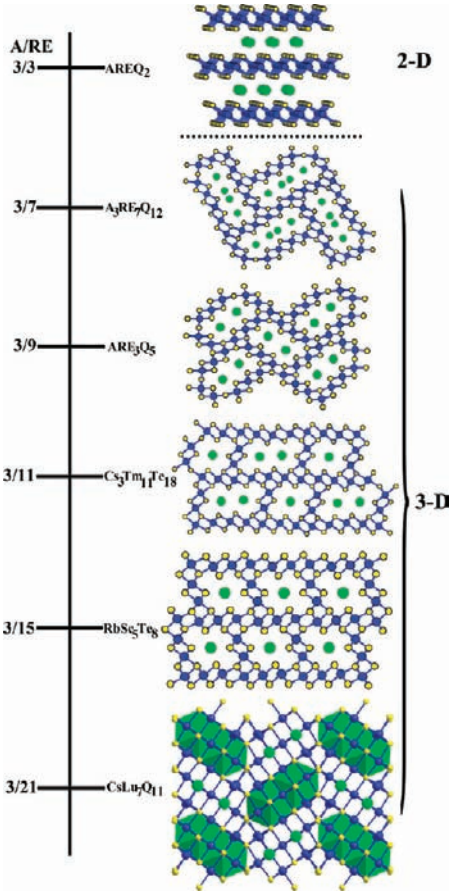

Figure 8. Relationship between the structure and the A/RE atomic ratio in the ternary A/RE/Q system. As the A/RE ratio increases (up), the structure changes a closed cavity structure to an open channel structure and then to a 2D layered structure. Yellow, Q; blue, RE; green, A; and green polyhedron, $Cs_2@Q_{18}$ dual tricapped cube.

channel structure with an infinite channel radius between the layers. The channel increase with the increase of the A/RE ratio has been clearly shown in Figure 8. This chart is useful to guide further exploration of unknown compounds with A/RE larger than 1 (only some oxides are known to date), less than 0.14, or between the denoted values, whose structure feature are expect to follow the trend to some degree.

Optical Properties. According to the diffuse-reflectance spectra at room temperature, the band gaps were estimated to be 1.86 eV for $Cs[Lu_7S_{11}]$ (Supporting Information, Figure S4a) and 1.78 eV for $Cs[Lu_7Se_{11}]$ (Supporting Information, Figure S4b), which are in agreement with their color and suggest the semiconductor behavior. These values are similar with those of $RbRESe_2$ (2.0−2.2 eV),[1] $KCeSe_4$ (1.54 eV),[23] and $KTbSe_4$ (1.65 eV).[23] Since $(ClCs_6)[RE_{21}Q_{34}]$ (RE = Dy, Ho; Q = S, Se, Te) are air and moisture sensitive, their properties cannot be measured under the current experimental conditions.

Electronic Structure. The band structures of $Cs[Lu_7Q_{11}]$ and $(ClCs_6)[Dy_{21}Se_{34}]$ are studied. The calculations indicate indirect band gaps and semiconductor characters, and the calculated E_g are 1.97, 1.38, and 1.44 eV for $Cs[Lu_7S_{11}]$, $Cs[Lu_7Se_{11}]$, and $(ClCs_6)[Dy_{21}Se_{34}]$, respectively, which agree well with the experimental results (Figures 9 and 10 and Figure S7 in the Supporting Information).

The distributions of states near E_F are similar for three compounds (Figures 9 and 10). The top of the valence bands is mostly made up of Q p states mixed with a small amount of the Lu/or Dy 5d states, whereas the bottom of the conduction bands consist mostly of Lu/or Dy 5d states and minor Q s states. Thus, the optical gap is likely determined by the electronic transitions from Q p states to Lu/or Dy 5d states. Therefore, these compounds have similar band gaps, and the difference comes from the different energy level of Q p states.

Note that the partial DOSs of Cs 6s states located almost above E_F, which proves that the Cs atom in all compounds acts primarily as an electron donor. Similarly, the Cl atom acts as an electron acceptor because its 3p states are located way below the E_F, which contributes to stabilize the structure of

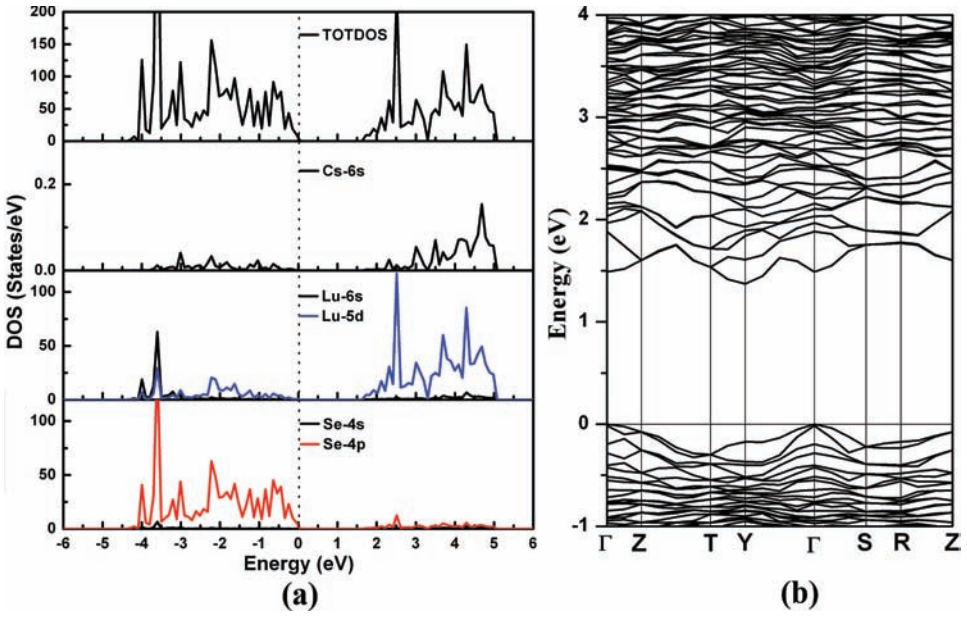

Figure 9. (a) Total and partial DOS and (b) band structure of $Cs[Lu_7Se_{11}]$. (Bands are shown only between −1.0 and 4.0 eV for clarity, and the Fermi level is set at 0 eV.)

dx.doi.org/10.1021/ic202494w | Inorg. Chem. 2012, 51, 4588−4596

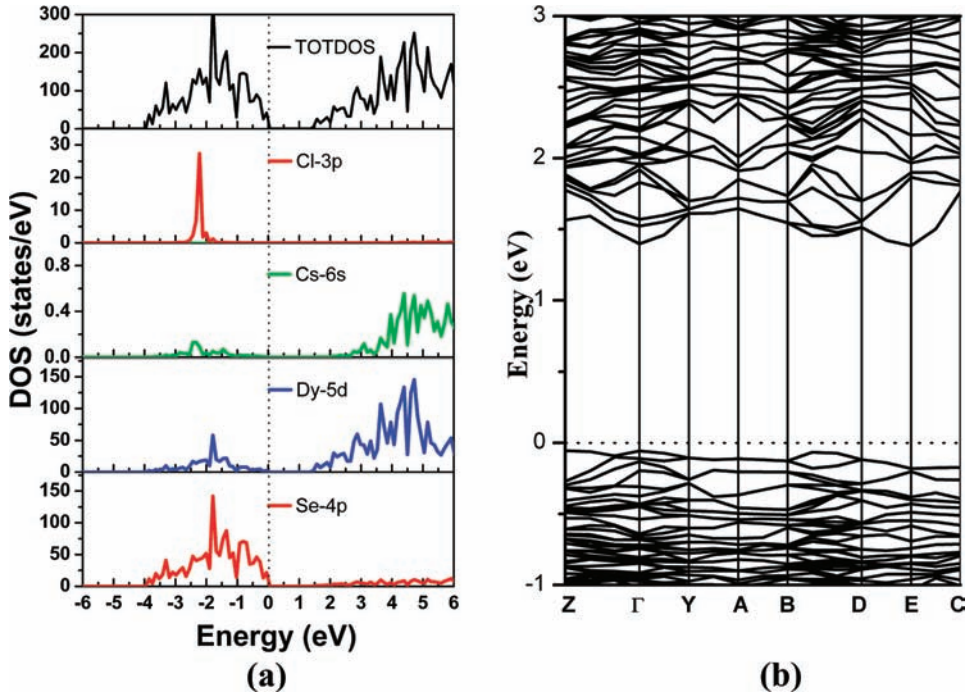

Figure 10. (a) Total and partial DOS and (b) band structure of $(ClCs_6)$ $[Dy_{21}Se_{34}]$. (Bands are shown only between −1.0 and 3.0 eV for clarity, and the Fermi level is set at 0 eV.)

$(ClCs_6)[Dy_{21}Se_{34}]$. Also the covalent bonding interactions between RE and Q atoms are pretty strong according to DOS.

CONCLUSION

Eight compounds, $Cs[Lu_7Q_{11}]$, $(ClCs_6)[RE_{21}Q_{34}]$, (RE = Dy, Ho; Q = S, Se, Te) representing two unprecedented structure types have been discovered by solid state reactions. Remarkably, diverse closed cavities of the $Cs_2@Q_{18}$ dual tricapped cube or the unprecedented $(ClCs_6)@Q_{32}$ matryoshka nesting doll structure are embedded with large intervals within the quasi-NaCl type RE−Q covalent matrix, respectively. The band structure studies suggest that the transitions from Q p states to RE 5d states determine the band gaps. Therefore these compounds have similar E_g, and the difference comes from the different energy level of Q p. More interestingly, these two types together with the majority of the known A/RE/Q compounds to illustrate a beautiful structure change trend. As the A/RE atomic ratio increases, the structure generally goes from a closed cavity structure to a channel structure and then to a 2D layered structure. Such a structure relationship may shed useful light on future explorations of possible compositions that are worth trying. Also the possible interesting physical properties that these closed cavity structures may possess is to be uncovered.

ASSOCIATED CONTENT

Supporting Information

CIF data and additional tables and figures. This material is available free of charge via the Internet at http://pubs.acs.org.

AUTHOR INFORMATION

Corresponding Author

*E-mail: chenl@fjirsm.ac.cn. Phone: (011)86-591-83704947.

Notes

The authors declare no competing financial interest.

ACKNOWLEDGMENTS

This research was supported by the National Natural Science Foundation of China under Projects 90922021, 20973175, and 21171168 and the "Knowledge Innovation Program of the Chinese Academy of Sciences" (Grant KJCX2-YW-H20).

REFERENCES

(1) Deng, B.; Ellis, D. E.; Ibers, J. A. *Inorg. Chem.* **2002**, *41*, 5716.
(2) Ohtani, T.; Honjo, H.; Wada, H. *Mater. Res. Bull.* **1987**, *22*, 829.
(3) Bronger, W.; Brüggemann, W.; Vonderahe, M.; Schmitz, D. *J. Alloys Compd.* **1993**, *200*, 205.
(4) Babo, J. M.; Schleid, T. *Z. Anorg. Allg. Chem.* **2009**, *635*, 1160.
(5) Stöwe, K.; Napoli, C.; Appel, S. *Z. Anorg. Allg. Chem.* **2003**, *629*, 1925.
(6) Keane, P. M.; Ibers, J. A. *Acta Crystallogr.* **1992**, *C48*, 1301.
(7) Bronger, W.; Eyck, J.; Kruse, K.; Schmitz, D. *Eur. J. Solid State Inorg. Chem.* **1996**, *33*, 213.
(8) Schleid, T.; Lissner, F. *Eur. J. Solid State Inorg. Chem.* **1993**, *30*, 829.
(9) Range, K. J.; Meister, W.; Klement, U. *Z. Kristallogr.* **1993**, *207*, 145.
(10) Lissner, F.; Hartenbach, I.; Schleid, T. *Z. Anorg. Allg. Chem.* **2002**, *628*, 1552.
(11) Kim, S. J.; Park, S. J.; Yun, H. S.; Do, J. W. *Inorg. Chem.* **1996**, *35*, 5283.
(12) Folchnandt, M.; Schleid, T. *Z. Anorg. Allg. Chem.* **1997**, *623*, 1501.
(13) Folchnandt, M.; Schleid, T. *Z. Anorg. Allg. Chem.* **1998**, *624*, 1595.
(14) Tougait, O.; Noël, H.; Ibers, J. A. *Solid State Sci.* **2001**, *3*, 513.
(15) Folchnandt, M.; Schleid, T. *Z. Kristallord.-New Cryst. Struct.* **2000**, *215*, 9.
(16) Yao, J. Y.; Deng, B.; Ellis, D. E.; Ibers, J. A. *J. Solid State Chem.* **2005**, *178*, 41.
(17) Babo, J. M.; Scheid, T. *Z. Anorg. Allg. Chem.* **2008**, *634*, 1463.
(18) Lemoine, P.; Tomas, A.; Carre, D.; Vovan, T.; Guittard, M. *Acta Crystallogr.* **1989**, *C45*, 350.

(19) Bensch, W.; Durichen, P. *Acta Crystallogr. C: Cryst. Struct. Commun.* **1997**, *53*, 267.
(20) Stöwe, K. *Solid State Sci.* **2003**, *5*, 765.
(21) Stöwe, K.; Napoli, C.; Appel, S. *Z. Anorg. Allg. Chem.* **2003**, *629*, 321.
(22) Stöwe, K. *J. Solid State Chem.* **2003**, *176*, 594.
(23) Sutorik, A. C.; Kanatzidis, M. G. *Chem. Mater.* **1997**, *9*, 387.
(24) Stöwe, K. *Z. Anorg. Allg. Chem.* **2003**, *629*, 403.
(25) Patschke, R.; Heising, J.; Schindler, J.; Kannewurf, C. R.; Kanatzidis, M. *J. Solid State Chem.* **1998**, *135*, 111.
(26) Brunn, H.; Hoppe, R. *Z. Anorg. Allg. Chem.* **1977**, *433*, 189.
(27) Hoch, C.; Bender, J.; Wohlfart, A.; Simon, A. *Z. Anorg. Allg. Chem.* **2009**, *635*, 1777.
(28) *CrystalClear*, version 1.3.5; Rigaku Corp.: The Woodlands, TX, 1999.
(29) Sheldrick, G. M. *SHELXTL*, version 5.1; Bruker-AXS: Madison, WI, 1998.
(30) Gelato, L. M.; Parthe, E. *J. Appl. Crystallogr.* **1987**, *20*, 139.
(31) Kortüm, G. *Reflectance Spectroscopy*; Springer-Verlag: New York, 1969.
(32) Kresse, G.; Furthmüller, J. *Phys. Rev. B* **1996**, *54*, 11169.
(33) Kresse, G.; Furthmüller, J. *Comput. Mater. Sci.* **1996**, *6*, 15.
(34) Perdew, J. P.; Wang, Y. *Phys. Rev. B* **1992**, *45*, 13244.
(35) Kresse, G.; Joubert, D. *Phys. Rev. B* **1999**, *59*, 1758.
(36) Blöchl, P. E. *Phys. Rev. B* **1994**, *50*, 17953.
(37) Blöchl, P. E.; Jepsen, O.; Andersen, O. K. *Phys. Rev. B* **1994**, *49*, 16223.
(38) Hulliger, F.; Hull, G. W. Jr. *Solid State Commun.* **1970**, *8*, 1374.
(39) Folchnandt, M.; Schneck, C.; Schleid, T. *Z. Anorg. Allg. Chem.* **2004**, *630*, 149.
(40) Dong, L.; Chen, H. S.; Xie, Z. *Angew. Chem., Int. Ed.* **2005**, *44*, 2128.
(41) Shannon, R. D. *Acta Crystallogr.* **1976**, *A32*, 751.
(42) Blackman, M.; Khan, I. H. *Proc. Phys. Soc.* **1961**, *77*, 471.
(43) Gaebell, H. C.; Meyer, G. *Z. Anorg. Allg. Chem.* **1984**, *515*, 133.